Photon-correlation measurements of stochastic limit cycles emerging from high-Q nonlinear silicon photonic crystal microcavities

N. Takemura,[*] M. Takiguchi ©, H. Sumikura ©, E. Kuramochi, A. Shinya, and M. Notomi

NTT Nanophotonics Center, NTT Corporation, 3-1, Morinosato Wakamiya Atsugi, Kanagawa 243-0198, Japan
and NTT Basic Research Laboratories, NTT Corporation, 3-1, Morinosato Wakamiya Atsugi, Kanagawa 243-0198, Japan

We performed measurements of the photon correlation [$g^{(2)}(\tau)$] in driven nonlinear high-Q silicon photonic crystal microcavities. The measured $g^{(2)}(\tau)$ exhibits damped oscillatory behavior when the input pump power exceeds a critical value. From a comparison between experiments and simulations, we attribute the measured oscillation of $g^{(2)}(\tau)$ to self-pulsing (a limit cycle) emerging from an interplay between the photon, carrier, and thermal dynamics. Namely, the oscillation frequency of $g^{(2)}(\tau)$ corresponds to the oscillation period of the limit cycle, while its finite coherence (damping) time originates from the stochastic nature of the limit cycle. From the standpoint of phase reduction theory, we interpret the measured coherence time of $g^{(2)}(\tau)$ as the coherence (diffusion) time of a generalized phase of the limit cycle. Furthermore, we show that an increase in laser input power enhances the coherence time of $g^{(2)}(\tau)$ up to the order of microseconds, which could be a demonstration of the stabilization of a stochastic limit cycle through pumping.

A limit cycle is a universal natural phenomenon observed in a variety of systems ranging from electrical circuits to biological systems. In particular, in living systems, limit cycles play fundamental roles as, for example, biochemical oscillators, including cell cycles and circadian clocks [1]. Importantly, as schematically shown on the left-hand side in Fig. 1(a), limit cycles exist only for nonlinear dissipative systems, and they are qualitatively different from periodic oscillations in conservative systems such as simple pendulums. For example, the orbit of a pendulum is determined by the initial condition and becomes unstable with perturbation, whereas a limit cycle has a stable orbit, which is an attractor independent of an initial condition but controlled by system parameters such as pump power. At the same time, dissipative systems are usually noisy environments. Therefore, biochemical oscillators work as stochastic limit cycles, and strategies to maintain the precision of stochastic biochemical oscillators have been actively investigated in theoretical biophysics and biochemistry [2–8]. In this direction, a novel strategy is to increase the amplitude of a limit cycle [2,3], which can be achieved by pumping [4] or by free-energy dissipation [5,7]. Furthermore, in discussing the precision of a limit cycle, a theoretical idea called a "phase reduction" proposed by Winfree and Kuramoto [9,10] plays a key role, which reduces the high-dimensional limit cycle dynamics to a one-dimensional "phase" dynamics along a limit cycle's orbit.

In this Rapid Communication, we report experimental investigations of stochastic limit cycles in the optical domain and demonstrate a strategy for stabilizing a stochastic limit cycle with pumping. Our system is based on a driven silicon (Si) photonic crystal (PhC) high-Q microcavity. A photonic microcavity device confines photons inside a nanoscale mode volume, which strongly enhances thermo-optic (TO) and carrier-induced optical nonlinearities in a medium such as a III-V material and Si [11–13]. Using the enhanced optical nonlinearity, optical bistability has been demonstrated with microcavities [14–19]. Furthermore, it is known that nonlinear photonic microcavities exhibit Hopf bifurcation, self-pulsing (a limit cycle) [20–26], and excitability [27,28]. In particular, in Refs. [27,28], not only excitability but also limit cycle oscillations have been demonstrated in driven PhC cavities. The advantages of using a photonic system include controllability of pump power and dissipation and ease of measurements, such as real-time and photon-correlation measurements. Therefore, photonic limit cycles could serve as artificial laboratories for understanding stochastic dynamical systems including biochemical oscillators. Furthermore, since optical limit cycles in all-Si PhC cavities operate at room temperature, it will be easy to integrate optical clocks in future silicon photonics circuits. In our study, we measured second-order photon-correlation functions [$g^{(2)}(\tau)$] for a light output of the driven cavity. When the laser input power exceeded a critical value, $g^{(2)}(\tau)$ exhibited damped oscillation. Together with numerical simulations, we show that the origin of the oscillation of $g^{(2)}(\tau)$ is self-pulsing (a limit cycle). Next, we argue that the finite coherence time of $g^{(2)}(\tau)$ originates from the stochastic nature of the system. The coherence time of $g^{(2)}(\tau)$ is interpreted as the coherence (diffusion) time of the generalized phase of the limit cycle [9,10]. By measuring the input power dependence of the coherence time of $g^{(2)}(\tau)$, we observed an enhancement of the phase coherence time up to the order of microseconds with an increase in input power. Finally, we discuss the observed enhancement of the phase coherence time as a general property of a limit cycle, namely, as a demonstration of the stabilization of a stochastic limit cycle through pumping [2–4,8].

_____
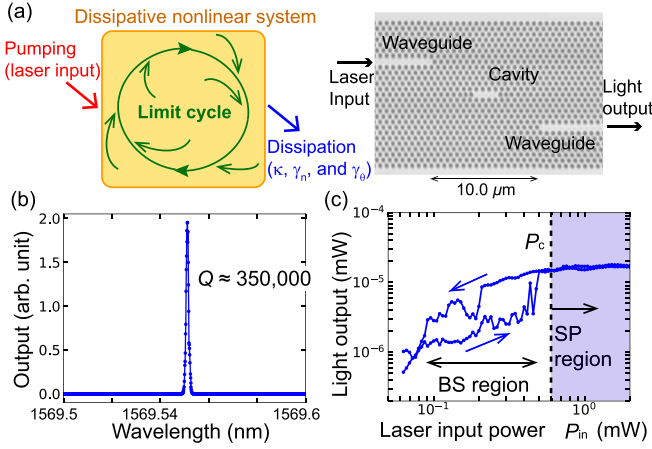*naotomo.takemura.ws@hco.ntt.co.jp

FIG. 1. (a) Illustration of a limit cycle emerging from a driven dissipative nonlinear system (left) and a laser scanning microscope image of the high-Q Si PhC microcavity (right). (b) Laser transmission spectrum of the cavity showing the resonance of a fundamental mode. (c) Output intensity I_{out} as a function of input power P_{in}, where P_c is the critical laser input power for self-pulsing. BS and SP represent bistable and self-pulsing regions, respectively. Here, P_{in} is the fiber output power of the tunable semiconductor laser.

On the right-hand side in Fig. 1(a) is an image of our device, which is based on a two-dimensional (2D) Si PhC slab with a cavity and two waveguides. The lattice constant, air-hole radius, and thickness of the PhC slab are 412, 100, and 215 nm, respectively. All the experiments were performed at room temperature. The cavity resonance of the fundamental mode is $\lambda_c = 1569.55$ nm, and the Q value is around 3.5×10^5 [see Fig. 1(b)]. The corresponding cavity photon lifetime, including losses to the waveguides, is around $1/\kappa = 300$ ps. This very high-Q value was achieved by using the ultrahigh-Q design proposed in Ref. [29], which omits three air holes and employs careful modulation of the surrounding air holes [for further details about the device, see Sec. I A in the Supplemental Material (SM) [30]]. We drive the cavity through the input waveguide with a tunable semiconductor laser, while we measure light outputs through the output waveguide. We introduce a normalized frequency detuning δ between the cavity resonance and laser input, which is defined as $\delta = (\omega_L - \omega_c)/\kappa$ with the cavity resonance frequency ω_c, the laser input frequency ω_L, and a field decay rate κ. In the measurements, we fixed the detuning as $\delta \simeq -2$. To measure second-order photon-correlation functions [$g^{(2)}(\tau)$], we employed superconducting nanowire single-photon detectors (SNSPDs) and a conventional start-stop Hanbury Brown–Twiss (HBT) interferometer. For real-time measurements, we used an avalanche photodiode (APD).

First, we discuss the bistable operation, which is shown in Fig. 1(c). When the detuning is $\delta \simeq -2$, the light output intensity I_{out} exhibits a hysteresis loop in terms of laser input power P_{in}. We use a negative detuning ($\delta \simeq -2$) to induce the transverse optical (TO) nonlinearity. The hysteresis loop shown in Fig. 1(c) is very noisy, which is probably because we performed a single-shot measurement by ramping the laser input power up and down slowly enough to induce the TO nonlinearity. The lower and upper thresholds of the bistable hysteresis loop are about $P_{in} = 0.08$ and 0.5 mW, respectively.

Note that the laser input power P_{in} was measured as the fiber output of the tunable semiconductor laser. If coupling loss from the fiber output and to the input waveguide is assumed to be 10 dB, the lower threshold power of bistability is 8 μW in the input waveguide, which is as low as that reported in our previous experiments [15,31]. Thus, the bistable operation in Fig. 1(c) is evidence of the onset of a high-Q cavity-enhanced optical nonlinearity induced by a very small input power. Here, the detailed shape of the hysteresis loop is not important, but the separation between the bistable and the self-pulsing region is important for observing the onset of self-pulsing, which was realized by the high-Q value of our cavity. This point is covered in more detail in the discussion of Fig. 3(a).

Second, for various laser input powers P_{in}, we measured the delay-dependent photon correlations $P_2(\tau)$ with the start-stop HBT interferometer, and attempted to reconstruct the normalized second-order photon correlation $g^{(2)}(\tau)$ from $P_2(\tau)$. $P_2(\tau)$ is a histogram of detected photon pairs in terms of the time delay τ. The upper part of Fig. 2(a) shows $P_2(\tau)$ for four laser input powers. The overall exponential decay of the measured $P_2(\tau)$ is a well-known artifact associated with the start-stop measurement [32]. Namely, when τ is longer, the probability of detecting photon pairs becomes smaller. Now, we define $g^{(2)}(\tau)$ as a classical intensity correlation $g^{(2)}(\tau) \equiv \langle I(t)I(t+\tau)\rangle/\langle I\rangle^2$, where the brackets represent statistical averages. For reconstructing normalized second-order photon-correlation functions $g^{(2)}(\tau)$, we fit the measured $P_2(\tau)$ as

$$P_2(\tau) \simeq C\big[1 + Ae^{-\frac{|\tau|}{\tau_r}}\cos(\omega_r|\tau|)\big]e^{-\frac{\tau}{\tau_{cor}}}, \qquad (1)$$

where $A \equiv g^{(2)}(0) - 1$, and C is another fitting parameter. Additionally, ω_r and τ_r are the oscillation frequency and coherence (damping) time of $g^{(2)}(\tau)$, respectively. On the other hand, τ_{cor} is the overall decay time of $P_2(\tau)$ associated with the start-stop counting method. With this fitting, we reconstruct $g^{(2)}(\tau)$ as $g^{(2)}(\tau) = g^{(2)}(0)\cos(\omega_r|\tau|)e^{-\tau/\tau_r}$. In the lower part of Fig. 2(a), we show four reconstructed $g^{(2)}(\tau)$'s corresponding to the four $P_2(\tau)$'s. When the laser input power is below a critical value, and even when it is in the bistable hysteresis loop, the light output has a Poissonian fluctuation, and thus $g^{(2)}(\tau) = 1$ as shown in Fig. 2(a) for $P_{in} = 0.6$ mW. Meanwhile, when the laser input power is above the critical value, $g^{(2)}(0)$ deviates from unity and $g^{(2)}(\tau)$ exhibits a damped oscillation [see $P_{in} = 1.3$ mW in Fig. 2(a)]. The critical laser input power of the damped oscillation of $g^{(2)}(\tau)$ was measured as $P_c \simeq 0.6$ mW, which is above the hysteresis loop as shown in Fig. 1(c). In Fig. 2(b), we plot the second-order photon correlation at a zero delay time $g^{(2)}(0)$ (top), the oscillation frequency ω_r (middle), and the coherence time τ_r (bottom) of $g^{(2)}(\tau)$. Figure 2(b) clearly shows that $g^{(2)}(0)$ deviates from unity when $P_{in} = P_c$. Additionally, the oscillation frequency ω_r has a maximum ($\omega_r/2\pi = 14$ MHz) when $P_{in} = P_c$, and it gradually decreases with an increase in laser input power. Meanwhile, for the coherence time τ_r, above P_c, τ_r increases with increasing laser input power (indicated by an arrow) and reaches a maximum value of 2.6 μs when $P_{in} \simeq 2.0$. However, when laser input power is increased further, the coherence time τ_r starts to decrease. The
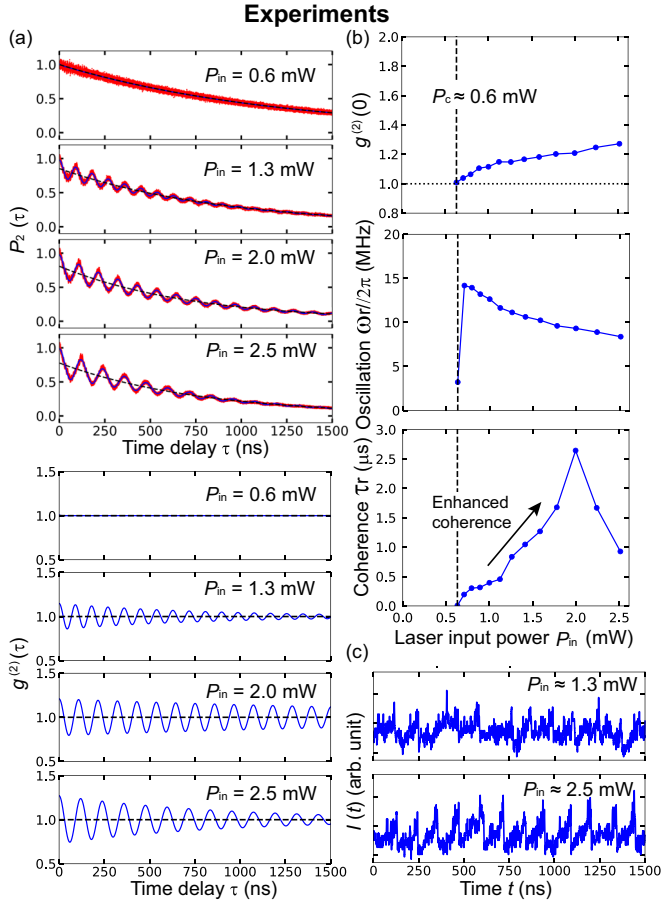
FIG. 2. (a) Examples of measured photon correlations with the start-stop HBT interferometer $P_2(\tau)$ with a fitting curve by Eq. (1) and reconstructed normalized second-order photon-correlation functions $g^{(2)}(\tau)$. (b) $g^{(2)}(0)$ (top), the oscillation frequency ω_r (middle), and the coherence time τ_r (bottom) of measured $g^{(2)}(\tau)$. The critical input power of self-pulsing is $P_c \simeq 0.6$ mW. (c) Real-time trajectories of the light output measured with an avalanche photodiode (APD) for two pump powers. For measurements, the detuning was fixed as $\delta \simeq -2$.

technical details of the hysteresis and $g^{(2)}(\tau)$ measurements are described in Sec. I C in the SM [30].

We attribute the origin of the oscillation of $g^{(2)}(\tau)$ to self-pulsation (a limit cycle) originating from Hopf bifurcation [20–22,24,27,28]. To confirm this, we performed real-time measurements of the light output. Figure 2(c) shows real-time trajectories of light outputs measured with the APD for two input powers above P_c, which clearly indicates real-time self-pulsation. Thus, here the origin of photon bunching [$g^{(2)}(0) > 1$] is the real-time modulation of light intensity [33], which is different from the photon bunching mechanism of chaotic light. Although we performed real-time measurements just to confirm limit cycle oscillation, in principle, we can calculate a classical $g^{(2)}(\tau)$ from the evolution of the light output. This alternative $g^{(2)}(\tau)$ measurement technique is discussed in Sec. I C in the SM [30].

Now, a new question arises: What is the origin of the finite coherence time of the observed $g^{(2)}(\tau)$? The answer is the stochastic (noisy) nature of our limit cycle. In fact, without

any noise, $g^{(2)}(\tau)$ will never decay and should have an infinite coherence time. For a deeper understanding of these experimental results, we performed numerical simulations based on the coupled-mode equations proposed in Refs. [19,34,35]. With the Kerr effects neglected, the normalized coupled-mode equations for an electric field α, normalized carrier density n, and thermal effect θ are given by

$$\dot{\alpha} = \kappa\{i(-\delta - \theta + n) - (1 + fn)\}\alpha + \kappa\sqrt{P_{\text{in}}}, \quad (2)$$

$$\dot{n} = \gamma_n\{-n + \xi|\alpha|^4\}, \quad (3)$$

$$\dot{\theta} = \gamma_\theta\{-\theta + \beta|\alpha|^2 + \eta|\alpha|^2 n\}. \quad (4)$$

Here, θ is proportional to the temperature difference between the cavity and the surrounding region [34]. Both n and θ are normalized to make constants of nonlinear energy shifts in Eq. (2) unity. The κ, γ_n, and γ_θ are decay rates of the electric field, carrier, and thermal effect, respectively. The field decay rate κ includes losses to the waveguides. P_{in} represents a normalized laser input power. The coefficients f, ξ, β, and η represent nonlinear effects associated with free-carrier absorption (FCA), two-photon absorption (TPA), heating with linear photon absorption, and FCA-induced heating, respectively. For these nonlinear coefficients, we use the same values as in Ref. [35]: $f = 0.0244$, $\xi = 8.2\kappa/\gamma_n$, $\beta = 0.0296\kappa/\gamma_\theta$, and $\eta = 0.0036\kappa/\gamma_\theta$, where the value of κ was estimated from the measured Q value. These nonlinear coefficients and their definitions are summarized on Tables S1 and S2 in the SM [30]. For the photon, carrier, and thermal lifetimes, we use $1/2\kappa = 300$ ps, $1/\gamma_n = 200$ ps, and $1/\gamma_\theta = 100$ ns, respectively. The fast carrier lifetime ($1/\gamma_n = 200$ ps) results from fast carrier diffusion associated with the small cavity of the PhC structure [14,36].

Before showing the simulations of stochastic dynamics, we briefly investigate the static properties of the deterministic coupled-mode equations (2)–(4). First, we attempt to obtain steady state values of α, n, and θ, which are denoted as α_s, n_s, and θ_s, respectively. By putting $\dot{\alpha} = 0$, $\dot{n} = 0$, and $\dot{\theta} = 0$ into Eqs. (2)–(4), we obtain an algebraic equation for $I_s = |\alpha_s|^2$ (see Sec. II B in the SM [30] for the explicit form of the algebraic equation). The system has two equilibria when the algebraic equation has two solutions for I_s. Second, at the steady state values of α_s, n_s, and θ_s, we calculate a Jacobian matrix and its eigenvalues to find self-pulsing (see Sec. II B in the SM [30] for the explicit form of the Jacobian and their eigenvalues). When a pair of the eigenvalues have positive real parts, the dynamical system becomes unstable, and Hopf bifurcation (self-pulsing) occurs [9,37]. Our system has the following three regions: a self-pulsing (SP) region where a single unstable equilibrium exists, a bistable (BS) region where there are two stable equilibria, and an SP + BS region where one equilibrium is stable and the other is not. The diagram of our dynamical system is shown in Fig. 3(a). We also found that bistability is induced solely by TO nonlinearity, while self-pulsing requires both carrier and TO nonlinearities (see Sec. II C in the SM [30]). The horizontal dashed line in Fig. 3(a) indicates that, for $\delta = -2$, with an increase in pump power, self-pulsing occurs when the input power reaches a critical power P_c, which is larger
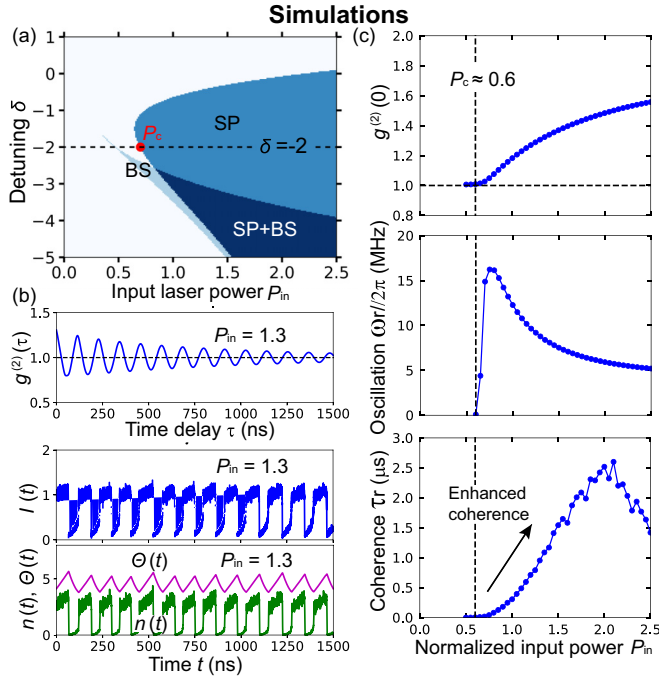
FIG. 3. (a) Simulated self-pulsing (SP) and bistable (BS) regions as a map of detuning δ and laser input power P_{in}, where the solid red circle represents the onset of SP for $\delta = -2$. (b) Simulated $g^{(2)}(\tau)$ and real-time evolution of carrier $n(t)$, thermal effect $\theta(t)$, and the light output $I(t) = |\alpha(t)|^2$ for $P_{in} = 1.3$. (c) $g^{(2)}(0)$ (top), oscillation frequencies ω_r (middle), and the coherence time τ_r (bottom) of the simulated $g^{(2)}(\tau)$. For simulations, the detuning $\delta = -2$ was used. The critical input power of self-pulsing is $P_c = 0.6$. While (a) is the result with the deterministic coupled-mode equations, (b) and (c) are the results with stochastic coupled-mode equations with noise terms.

than the upper threshold of the bistable hysteresis loop. This is consistent with our measurement shown in Fig. 1(c). We comment on the importance of the separation between the SP and BS regions shown in Fig. 1(c). In our experiment, we were able to observe the onset (bifurcation point) of self-pulsing outside the hysteresis loop with moderate negative detuning ($\delta \simeq -2$) and low input power ($P_c \simeq 0.6$ mW). We found that as the photon lifetime increases (a Q value increases), the SP region separates from the BS region, and self-pulsing occurs with a near-zero detuning and low input power. Thus, a high-Q value is technically very important for the observation of the onset of self-pulsing. A further discussion on the impact of Q on self-pulsing is given in Sec. III in the SM [30], where simulations for a moderate $Q = 2.0 \times 10^4$ value are shown. Even in the moderate Q cavity, nontrivial regions are only the SP, BS, and SP + BS regions in the same way as in Fig. 3(a). However, the shapes of these regions as functions of δ and P are very different from those in Fig. 3(a).

Now, we investigate the dynamical properties of coupled-mode equations (2)–(4). Since we are interested in a fluctuating system, we add additive Langevin noises f_x and f_y only to Eq. (4), where we assume that field and laser input noises are dominant over other noises. Actually, we find that the inclusion of carrier and thermal noises does not

qualitatively modify the results. The noise terms satisfy the correlations $\langle f_i(t) f_j(t') \rangle = 2D_\alpha \delta_{i,j} \delta(t - t')$ and $\langle f_i(t) \rangle = 0$, where $i(j) = x, y$ and the coefficient D_α is the strength of the noise. For numerical simulations of the stochastic equations, we employed the Euler-Maruyama method. The value of the noise strength was set as $\sqrt{2D_\alpha} = 0.05\sqrt{\kappa}$, which was chosen to reproduce the observed maximum coherence time of $g^{(2)}(\tau)$ [38]. Figure 3(b) shows simulated $g^{(2)}(\tau)$, $n(t)$, $\theta(t)$, and $I(t) = |\alpha(t)|^2$ for input power $P_{in} = 1.3$, which clearly reproduce the damped oscillatory behavior of $g^{(2)}(\tau)$ and the real-time self-pulsing when the input power is above the critical input power $P_c = 0.6$. Additionally, in Fig. 3(c), we plot $g^{(2)}(0)$ (top), the oscillation frequency ω_r (middle), and the coherence time τ_r (bottom) of $g^{(2)}(\tau)$ as a function of P_{in}, which also qualitatively reproduce the measurements shown in Fig. 2(b). Namely, the simulation reproduces the monotonic decrease of ω_r and the enhancement and reduction of the coherence time τ_r with an increase in pump power. Here, we briefly comment on the reduction of the coherence time τ_r in the high input power region ($P_{in} > 2.0$ mW in the experiment). We found that field and carrier noises give rise to the coherence reduction, while thermal noise does not. Simulations with carrier and thermal noises are shown in Sec. IV in the SM [30], which indicates that the thermal noise may be negligible.

In the rest of this Rapid Communication, we focus on the region around the critical input power of self-pulsing and attempt to interpret the enhancement of the coherence time τ_r, which is indicated by an arrow in the bottom graphs of Fig. 2(b) (experiment) and Fig. 3(c) (simulation). For this purpose, we employ the phase reduction theory, which starts from defining a generalized phase ϕ along a limit cycle orbit. Importantly, in phase reduction, noises in a limit cycle are reduced to a frequency drift and a phase noise as $\dot{\phi} = \omega + v + f_\phi$, where ω, v, and f_ϕ represent the original frequency of a limit cycle, the frequency drift, and the phase noise, respectively [9,10]. The phase noise f_ϕ satisfies correlations $\langle f_\phi(t) f_\phi(t') \rangle = 2D_\phi \delta(t - t')$ and $\langle f_\phi(t) \rangle = 0$, where D_ϕ is the phase diffusion rate. Therefore, for a limit cycle, noises are interpreted as diffusion of the generalized phase. Furthermore, the coherence time of a correlation function such as $g^{(2)}(\tau)$ corresponds to the coherence (diffusion) time of the generalized phase: $\tau_r \simeq 1/D_\phi$ [5,7].

To be more concrete, let us recall that for the stochastic Stuart-Landau model without phase-amplitude coupling, the phase diffusion rate well above Hopf bifurcation is approximated as [5,7,39–41]

$$D_\phi \propto D_0/P_{in}, \tag{5}$$

where D_0 is the strength of noises, while P_{in} represents the pump or input power to the system. If D_0 is constant, Eq. (5) represents the suppression of phase diffusion by pumping [42]. Additionally, Ref. [5] shows that Eq. (5) can also be written with a free-energy dissipation rate ΔW as $D_\phi \propto \Delta W^{-1}$, which means the suppression of phase diffusion through free-energy dissipation. Furthermore, Eq. (5) is intuitively understood as a one-dimensional diffusion process along an orbit of a limit cycle [43]. Thus, if the noise strength D_0 is constant, the longer the orbit's circumference,

the longer is the time required for the phase to diffuse over 2π. Additionally, the amplitude and the circumference length generally increase with pumping P_{in} in the vicinity of Hopf bifurcation. Thus, the essence of Eq. (5) lies in the fixed strength of noises and the increase in the amplitude by pumping. In particular, the latter is possible only for limit cycles. Thus, in the vicinity of a critical point of self-pulsing, an enhancement of phase coherence will generally occur for any limit cycle, including ours.

In summary, we performed photon-correlation measurements of stochastic limit cycles using a driven high-Q silicon photonic crystal cavity. We observed the damped oscillation of photon correlation associated with self-pulsing (a limit cycle). Furthermore, by increasing the input power, the coherence time of the photon-correlation function was enhanced up to the order of microseconds, which could be interpreted as a coherence time enhancement of a generalized phase through pumping.

Note added. Recently, we became aware of Ref. [44], which discusses similar topics to ours.

[1] B. Novák and J. J. Tyson, Nat. Rev. Mol. Cell Biol. **9**, 981 (2008).

[2] P. Gaspard, J. Chem. Phys. **117**, 8905 (2002).

[3] D. Gonze, J. Halloy, and P. Gaspard, J. Chem. Phys. **116**, 10997 (2002).

[4] H. Qian, J. Phys. Chem. B **110**, 15063 (2006).

[5] Y. Cao, H. Wang, Q. Ouyang, and Y. Tu, Nat. Phys. **11**, 772 (2015).

[6] A. C. Barato and U. Seifert, Phys. Rev. X **6**, 041053 (2016).

[7] C. Fei, Y. Cao, Q. Ouyang, and Y. Tu, Nat. Commun. **9**, 1434 (2018).

[8] B. Nguyen, U. Seifert, and A. C. Barato, J. Chem. Phys. **149**, 045101 (2018).

[9] Y. Kuramoto, *Chemical Oscillations, Waves, and Turbulence* (Courier Corporation, North Chelmsford, MA, 2003).

[10] H. Nakao, Contemp. Phys. **57**, 188 (2016).

[11] P. E. Barclay, K. Srinivasan, and O. Painter, Opt. Express **13**, 801 (2005).

[12] T. Uesugi, B.-S. Song, T. Asano, and S. Noda, Opt. Express **14**, 377 (2006).

[13] J. Leuthold, C. Koos, and W. Freude, Nat. Photonics **4**, 535 (2010).

[14] T. Tanabe, M. Notomi, S. Mitsugi, A. Shinya, and E. Kuramochi, Opt. Lett. **30**, 2575 (2005).

[15] M. Notomi, A. Shinya, S. Mitsugi, G. Kira, E. Kuramochi, and T. Tanabe, Opt. Express **13**, 2678 (2005).

[16] T. Tanabe, A. Shinya, E. Kuramochi, S. Kondo, H. Taniyama, and M. Notomi, Appl. Phys. Lett. **91**, 021110 (2007).

[17] E. Weidner, S. Combrié, A. de Rossi, N.-V.-Q. Tran, and S. Cassette, Appl. Phys. Lett. **90**, 101118 (2007).

[18] L.-D. Haret, T. Tanabe, E. Kuramochi, and M. Notomi, Opt. Express **17**, 21108 (2009).

[19] A. de Rossi, M. Lauritano, S. Combrié, Q. V. Tran, and C. Husko, Phys. Rev. A **79**, 043818 (2009).

[20] G. Priem, P. Dumon, W. Bogaerts, D. V. Thourhout, G. Morthier, and R. Baets, Opt. Express **13**, 9623 (2005).

[21] T. J. Johnson, M. Borselli, and O. Painter, Opt. Express **14**, 817 (2006).

[22] W. H. P. Pernice, M. Li, and H. X. Tang, Opt. Express **18**, 18438 (2010).

[23] S. Malaguti, G. Bellanca, A. de Rossi, S. Combrié, and S. Trillo, Phys. Rev. A **83**, 051802(R) (2011).

[24] N. Cazier, X. Checoury, L.-D. Haret, and P. Boucaud, Opt. Express **21**, 13626 (2013).

[25] A. M. Yacomotti, S. Haddadi, and S. Barbay, Phys. Rev. A **87**, 041804(R) (2013).

[26] Y. Yu, W. Xue, E. Semenova, K. Yvind, and J. Mork, Nat. Photonics **11**, 81 (2017).

[27] A. M. Yacomotti, P. Monnier, F. Raineri, B. B. Bakir, C. Seassal, R. Raj, and J. A. Levenson, Phys. Rev. Lett. **97**, 143904 (2006).

[28] M. Brunstein, A. M. Yacomotti, I. Sagnes, F. Raineri, L. Bigot, and A. Levenson, Phys. Rev. A **85**, 031803(R) (2012).

[29] E. Kuramochi, E. Grossman, K. Nozaki, K. Takeda, A. Shinya, H. Taniyama, and M. Notomi, Opt. Lett. **39**, 5780 (2014).

[30] See Supplemental Material at http://link.aps.org/supplemental/10.1103/PhysRevA.102.011501 for the detailed descriptions of the experimental setup, theoretical model, simulations for a moderate Q value, and carrier and thermal noise effects.

[31] T. Tanabe, M. Notomi, E. Kuramochi, A. Shinya, and H. Taniyama, Nat. Photonics **1**, 49 (2007).

[32] L. Mandel and E. Wolf, *Optical Coherence and Quantum Optics* (Cambridge University Press, Cambrdige, UK, 1995).

[33] R. Loudon, Rep. Prog. Phys. **43**, 913 (1980).

[34] T. Van Vaerenbergh, M. Fiers, J. Dambre, and P. Bienstman, Phys. Rev. A **86**, 063808 (2012).

[35] L. Zhang, Y. Fei, T. Cao, Y. Cao, Q. Xu, and S. Chen, Phys. Rev. A **87**, 053805 (2013).

[36] T. Tanabe, H. Taniyama, and M. Notomi, J. Lightwave Technol. **26**, 1396 (2008).

[37] S. H. Strogatz, *Nonlinear Dynamics and Chaos: With Applications to Physics, Biology, Chemistry, and Engineering* (CRC Press, Boca Raton, FL, 2018).

[38] In actual numerical simulations, we introduce the noise to a difference equation as $\sigma \xi_R \sqrt{dt}$, where $\sigma = 0.05\sqrt{\kappa}$ and ξ_R is a random number following the normal distribution $N(0, 1)$.

[39] Louisell, *Quantum Statistical Properties of Radiation*, Vol. 7 (Wiley, New York, 1973).

[40] N. G. Van Kampen, *Stochastic Processes in Physics and Chemistry*, Vol. 1 (Elsevier, Amsterdam, 1992).

[41] H. Risken, in *The Fokker-Planck Equation* (Springer, Berlin, 1996), pp. 63–95.

[42] One may find that Eq. (5) is analogous to the well-known Schawlow-Townes linewidth reduction in laser physics.

[43] M. O. Scully and M. S. Zubairy, *Quantum Optics* (Cambridge University Press, Cambridge, UK, 1999).

[44] M. Marconi, F. Raineri, A. Levenson, A. M. Yacomotti, J. Javaloyes, S. H. Pan, A. El Amili, and Y. Fainman, Phys. Rev. Lett. **124**, 213602 (2020).